Sulfate reducing bacteria are active and co-occur with diatoms during a spring phytoplankton bloom

Siebers, R.[1], Schultz, D.[1], Farza, M. S.[1], Brauer, A.[1], Zühlke, D.[1], Hoff, K.[1], Mücke, P. A[1], Wang, F.[2], Bernhardt, J.[1], Teeling, H.[2], Becher, D.[1], Riedel, K.[1,3], Urich, T.[1,3], Bengtsson, M. M.[1, 3]

Affiliations

1: Institute of Microbiology, University of Greifswald, Greifswald, Germany

2: Max Planck Institute for Marine Microbiology, Bremen, Germany

3: Institute of Marine Biotechnology, Greifswald, Germany

Corresponding author:

Mia M. Bengtsson

mia.bengtsson@uni-greifswald.de

ABSTRACT

Phytoplankton blooms fuel marine food webs with labile dissolved carbon, but also lead to the formation of particulate organic matter composed of living and dead algal cells. These particles are sites of intense algal-bacterial interactions and provide diverse niches for microbes to thrive. We analyzed co-occurrence networks based on 16S and 18S ribosomal RNA gene amplicon sequences obtained during a spring phytoplankton bloom in the North Sea. Particulate fractions larger than 10 µm diameter were collected at almost daily intervals between early March and late May in 2018. Metaproteomics was used to assess microbial functional activity at three selected time points during the sampling period. Network analysis identified two major modules representing bacteria co-occurring with diatoms and with dinoflagellates, respectively. Bacterial communities associated with these two algal lineages differed in composition, with diatoms distinctly clustering with known sulfate-reducing *Desulfobacterota* as well as with potentially sulfur-oxidizing *Ectothiorhodospiraceae*. Metaproteomics confirmed the presence of key enzymes involved in dissimilatory sulfate reduction, a process known to occur in sinking particles at greater depths, but considered of lesser importance in the photic zone. However, our results suggest presence of sufficiently

anoxic niches in diatom-derived particles, which may have implications for diatom-bacterial interactions and carbon export during phytoplankton blooms.

INTRODUCTION

Phytoplankton blooms represent primary productivity hotspots, which inject gigatons of organic carbon into coastal oceans every year. It has been estimated that over 90% of algal-produced carbon is consumed by heterotrophic bacteria in the immediate vicinity of algal cells, the phycosphere, during typical bloom situations (Seymour et al. 2017). Some of these bacteria are directly associated with living algal cells, or with sinking aggregates of senescent or dead algae, and therefore play an important role in the biological carbon pump. Despite their importance in global carbon cycling, particle-associated (PA) bacterial communities are less well understood than their free-living counterparts. In fact, they are often overlooked due to the common practice of pre-filtration to exclude larger organisms prior to community composition analyses.

A defining feature of marine particles are the steep chemical and redox gradients that PA bacterial communities are exposed to compared to free-living, planktonic bacteria. These gradients have been intensively studied in the context of bathypelagic sinking particles (i.e., marine snow), which harbor anoxic micro-niches enabling microbial sulfate reduction and denitrification (Bianchi et al. 2018, Raven et al. 2021). In the photic zone, these micro-niches are considered less important, especially for oxygen-producing living algal cells. Aggregates of living algae are rather known for a diverse microbiome of aerobic, heterotrophic bacteria that degrade complex algal organic matter, such as polysaccharide-rich exudates. These bacteria are selected by factors such as host genotype (Ahern et al. 2021), the surrounding environment (Barreto Filho et al. 2021) and via stochastic processes (Stock et al. 2022). It is methodologically challenging to study associations between algal and bacterial taxa during natural phytoplankton blooms by direct observations, (i) due to the transient nature of these associations, and (ii) due to the innate complexities and dynamics of algal and bacterial communities during bloom events. Temporal co-occurrence analysis offers an indirect way to infer algae-bacteria associations that reduces complexity and thereby enables generating hypotheses about specific interactions and their potential functional implications.

We investigated associations (co-occurrence) of PA bacterial and algal taxa during a spring phytoplankton bloom in the southern North Sea at the long-term ecological research site Helgoland Roads (Wiltshire 2010) in the year 2018. We aimed to identify PA bacterial taxa potentially interacting with diatoms during the bloom. Using 16S and 18S rRNA gene amplicon data from a well-resolved time series (near daily sampling) collected between early March and late May in 2018, we constructed co-occurrence networks focusing exclusively on bacteria-eukaryote co-occurrences (Bengtsson et al. 2017) in particles larger than 10 µm. In addition, we addressed bacterial functional gene expression by analysis of metaproteomes (Schultz et al. 2020) from three selected timepoints during the bloom (Fig. 1).

RESULTS & DISCUSSION

The spring phytoplankton bloom in 2018 was characterized by an initial dominance of diatoms (*Bacillariophyceae*), followed by an increase in dinoflagellate (*Dinophyceae*) relative abundances after the bloom peak (peak in Chlorophyll a concentration, Fig. 1). Co-occurrence analysis resulted in distinct network modules around diatoms and dinoflagellates. Based on significant positive correlations (Spearman rho>0.7, corrected p>0.01) between eukaryotic 18S rRNA gene amplicon sequence variants (ASVs) and prokaryotic 16S rRNA gene ASVs, including all 51 sampled timepoints during the 2018 spring bloom, the network consisted of three distinct modules (Fig. 2a). Two of these modules were dominated by eukaryotic ASVs belonging to diatoms and dinoflagellates, respectively, while the third module mostly contained diatom ASVs and was linked to the dinoflagellate-dominated network module. These network modules roughly corresponded to the phytoplankton taxa prevalent in the early stages of the bloom (module I, mainly diatoms), during the late stages of the bloom (module II, mainly dinoflagellates) and mid-bloom around peak chlorophyll *a* (module III, Fig. 1).

Several ASVs belonging to the *Desulfobacterota* were part of the main diatom - dominated network module I. Although *Desulfobacterota* have not been identified as frequent members of diatom microbiomes in either cultures or in the field so far (Helliwell et al. 2022), a recent global survey of the diatom interactome detected positive correlations between diatoms and sulfate-reducing bacteria in samples from the Tara Oceans expedition (Vincent & Bowler 2020). *Desulfobacterota* ASVs were only positively correlated with diatoms and not with dinoflagellates in our study (Fig. 2b. In addition, ASVs classified as

95 *Ectothiorhodospiraceae* also co-occurred with diatoms. These purple sulfur bacteria
96 (belonging to *Gammaproteobacteria*) are anaerobic to microaerophilic (Imhoff 2022), and can
97 oxidize H_2S, e.g., produced via dissimilatory sulfate reduction by members of the
98 *Desulfobacterota*. This observation is consistent with potential sulfur cycling in close
99 association with diatoms during this phytoplankton bloom under anoxic to very low oxygen
100 conditions.

101 Co-occurrence of diatom- and *Desulfobacterota* rRNA genes does not in itself indicate
102 that sulfate reduction is taking place in diatom-derived particles in the photic zone. Therefore,
103 we used metaproteomics to search for actively expressed key functional genes. We detected
104 4,584 protein groups in > 10 µm filter fractions from three sampled timepoints (see Fig. 1,
105 Figures S4 and S5) during the bloom. Of these, 22 were classified as belonging to different
106 *Desulfobacterota* orders, (Table S1). The relative abundance of predicted *Desulfobacterota*
107 proteins in the metaproteome was 0.18% (expressed as normalized spectral abundance factor
108 - NSAF). This order of magnitude corresponded well to the relative abundance of
109 *Desulfobacterota* ASVs in the microbiome at the same timepoints (average 0.38%, Fig S1).
110 Remarkably, no less than 18% of the *Desulfobacterota* metaproteome fraction (in terms of
111 protein abundance) consisted of key enzymes for dissimilatory sulfate reduction (Fig. 2c).
112 Both the alpha and the beta subunits of dissimilatory sulfite reductase (DSR) were detected.
113 Furthermore, adenylyl-sulfate (adenosine-5'-phosphosulfate) reductase (APS reductase), was
114 also detected in three instances. Only ATP sulfurylase, the third key enzyme of the
115 dissimilatory sulfate reduction pathway, was not detected. We used a conservative threshold
116 for protein identification of at least two matching peptides to consider a protein as validly
117 detected. Therefore, the detection of dissimilatory sulfate reduction key enzymes provides a
118 strong indication that the diatom-associated *Desulfobacterota* were actively carrying out
119 sulfate reduction, and thus gaining energy through anaerobic respiration.

120 Our results highlight the complexity of algal-bacterial interactions during
121 phytoplankton blooms and corroborate the need to study algae-bacteria particles as spatially
122 heterogeneous entities. Our observations lead us to hypothesize that living diatom-derived
123 particles provide sufficiently anoxic niches, at least during parts of the day-night cycle, to
124 sustain anaerobic sulfur cycling in the photic zone. Diatoms, such as *Thallassiosira* spp. and
125 *Thalassionema* spp., which were co-occurring with *Desulfobacterota* in this study (Fig. 2a), are
126 known to form aggregates (Thornton 2002). For example, several species of *Thalassiosira*

127 extrude long chitin fibrils, which prevent sinking and bind exopolymeric substances (EPS) also
128 produced by the algal cells (Den et al. 2023, Herth & Barthlott 1979). This creates a favorable
129 environment for bacteria to attach, which can in turn stimulate algal EPS production (Gärdes
130 et al. 2011). EPS makes particles adhesive and thus bacteria can be captured in this sticky EPS
131 layer. This includes suspended benthic bacteria, which may be abundant in shallow areas such
132 as the Helgoland sampling site (6-10 m depth depending on tide).

133 Smaller particles can aggregate to larger particles by collision and adhesion, in
134 particular during phytoplankon blooms with high particle densities. Such aggregates can
135 feature high numbers of living, photosynthesizing algal cells (Thornton 2002). These cells
136 produce ample oxygen during the day, but at night respiration by the algal cells and their
137 surrounding bacteria may deplete oxygen sufficiently for low oxygen or even anaerobic micro-
138 niches to form. Our data suggest that these micro-niches can support microbial sulfate
139 reduction in diatom microbiomes. The latter may thus be as complex as those of animals and
140 other multicellular organisms, featuring distinct micro-niches with sub-microbiomes
141 (analogous to e.g., human skin vs. gut microbiomes), whose compositions depend on the
142 chemical environment on a small spatial scale. Anoxic micro-niches in diatom-derived
143 aggregates may even affect the biological carbon pump insofar, as sulfate reduction can
144 chemically alter particulate organic matter, rendering it resistant to microbial degradation
145 (Raven et al. 2021).

146 Temporal associations, such as detected by our co-occurrence network analyses, have
147 to be interpreted with caution as additional variable factors that were not taken into account
148 may influence the resulting correlations. For example, we cannot completely rule out an
149 influence of underlying sediment microbiomes at the rather shallow sampling site, which may
150 become resuspended during times of heavy wind thereby introducing anaerobic microbes to
151 the pelagic environment. However, we did not find a clear link between wind conditions,
152 Secchi depth, and *Desulfobacterota* in this study (Fig. S2). Further, the diatom taxa co-
153 occurring with *Desulfobacteria* were also primarily classified as common pelagic genera such
154 as *Thalassiosira* and *Thalassionema*. Limitations notwithstanding, co-occurrence network
155 analysis provides a tool for formulating hypotheses about interactions between taxa that can
156 be tested experimentally in future investigations.

157 We showed that there was a temporal association between diatom and bacterial taxa
158 belonging to the *Desulfobacterota* during a North Sea phytoplankton spring bloom and that

key enzymes involved in sulfate reduction by these bacteria were expressed during the same bloom. However, a physical association between these bacteria and diatoms was not proven by our approach and would require *in situ* microscopic investigation using for example taxon- or gene- specific fluorescent probes. Likewise, it has yet to be investigated, whether such temporal and physical associations are annually recurrent, under what specific conditions they occur, and which specific diatom taxa are involved. The presence of anaerobic niches inside aggregates of living diatoms provides a new facet of algal-bacterial-organic matter interactions in the photic zone, with potential implications for carbon export from phytoplankton blooms.

DATA AVAILABILITY

Metagenome raw reads and assembled contigs used for metaproteome assignment are publicly available at the European nucleotide archive under the project accession number PRJEB38290. 16S- and 18S-rRNA gene amplicon data are also available via ENA under the project accession number PRJEB51816. Mass spectrometry proteomics data have been deposited to the ProteomeXchange Consortium via the PRIDE (Perez-Riverol et al., 2022), repository with dataset identifier PXD035982. Original mass spectrometry proteomics data can be accessed for review (**Username:** reviewer_pxd035982@ebi.ac.uk **Password:** umim4qCW) and will be made publically available upon manuscript acceptance.

ACKNOWLEDGEMENTS

We thank the team from the Biological Station Helgoland (BAH-AWI, Germany) and the captains and crews from FS Aade and FS Uthörn for help with sampling, analyses, logistics, and providing lab space. The Helgoland Time Series is supported by the Helmholtz Association as an LK-II performance category program. This study was funded by the Deutsche Forschungsgemeinschaft (DFG) in the framework of the research unit FOR2406 'Proteogenomics of Marine Polysaccharide Utilization (POMPU)' by grants of KR/MB (RI 969/9-2), DB (BE 3869/4-2) and HT (TE 813/2-2).

188 CONFLICT OF INTEREST

189 The authors declare no conflicts of interest

190

191 REFERENCES

192 Ahern OM, Whittaker KA, Williams TC, Hunt DE, Rynearson TA. Host genotype structures the
193 microbiome of a globally dispersed marine phytoplankton. Proc Natl Acad Sci U S A 2021.
194 doi:10.1073/pnas.2105207118.

195 Barreto Filho MM, Walker M, Ashworth MP, Morris JJ. Structure and Long-Term Stability of the
196 Microbiome in Diverse Diatom Cultures. Microbiol Spectr. 2021;9(1):e0026921.
197 doi:10.1128/Spectrum.00269-21.

198 Bengtsson MM, Bühler A, Brauer A, Dahlke S, Schubert H, Blindow I. Eelgrass Leaf Surface Microbiomes
199 Are Locally Variable and Highly Correlated with Epibiotic Eukaryotes. Front Microbiol.
200 2017;8:1312. doi:10.3389/fmicb.2017.01312.

201 Bianchi D, Weber TS, Kiko R, Deutsch C. Global niche of marine anaerobic metabolisms expanded by
202 particle microenvironments. Nature Geosci. 2018;11(4):263–8. doi:10.1038/s41561-018-0081-0.

203 Den TQ, Neu TR, Sultana S, Giebel HA, Simon M, Billerbeck S. Distinct glycoconjugate cell surface
204 structures make the pelagic diatom Thalassiosira rotula an attractive habitat for bacteria. Journal
205 of Phycology 2023. http://doi.org/10.1111/jpy.13308

206 Gärdes A, Iversen MH, Grossart H-P, Passow U, Ullrich MS. Diatom-associated bacteria are required
207 for aggregation of *Thalassiosira weissflogii*. ISME J. 2011;5(3):436–45.
208 doi:10.1038/ismej.2010.145.

209 Helliwell KE, Shibl AA, Amin SA. The Diatom Microbiome: New Perspectives for Diatom-Bacteria
210 Symbioses. In: Falciatore A, Mock T, eds. The Molecular Life of Diatoms. Cham: Springer
211 International Publishing; 2022. p. 679–712. doi:10.1007/978-3-030-92499-7_23.

212 Herth W, & Barthlott W. The site of beta-chitin fibril formation in centric diatoms. I. Pores and fibril
213 formation. Journal of Ultrastructure Research, 1979; 68(1), 6–15. http://doi.org/10.1016/s0022-
214 5320(79)90137-0

215 Imhoff JF, Kyndt JA, Meyer TE. Genomic Comparison, Phylogeny and Taxonomic Reevaluation of the
216 *Ectothiorhodospiraceae* and Description of *Halorhodospiraceae* fam. nov. and *Halochlorospira*
217 gen. nov. Microorganisms 2022. doi:10.3390/microorganisms10020295.

218 Raven MR, Keil RG, Webb SM. Microbial sulfate reduction and organic sulfur formation in sinking
219 marine particles. Science. 2021;371(6525):178–81. doi:10.1126/science.abc6035.

220 Schultz D, Zühlke D, Bernhardt J, Francis TB, Albrecht D, Hirschfeld C, et al. An optimized
221 metaproteomics protocol for a holistic taxonomic and functional characterization of microbial

222 communities from marine particles. Environ Microbiol Rep. 2020;12(4):367–76.
223 doi:10.1111/1758-2229.12842.
224 Seymour JR, Amin SA, Raina J-B, Stocker R. Zooming in on the phycosphere: the ecological interface
225 for phytoplankton-bacteria relationships. Nat Microbiol. 2017;2:17065.
226 doi:10.1038/nmicrobiol.2017.65.
227 Stock W, Willems A, Mangelinckx S, Vyverman W, Sabbe K. Selection constrains lottery assembly in
228 the microbiomes of closely related diatom species. ISME COMMUN. 2022. doi:10.1038/s43705-
229 022-00091-x.
230 Thornton DCO. Diatom aggregation in the sea: mechanisms and ecological implications. Euro. J.
231 Phycol. 2002;37(2):149–61. doi:10.1017/S0967026202003657.
232 Vincent F, Bowler C. Diatoms Are Selective Segregators in Global Ocean Planktonic Communities.
233 mSystems 2020. doi:10.1128/mSystems.00444-19.
234 Wiltshire KH, Kraberg A, Bartsch I, Boersma M, Franke H-D, Freund J, et al. Helgoland Roads, North
235 Sea: 45 Years of Change. Estuaries and Coasts. 2010;33(2):295–310. doi:10.1007/s12237-009-
236 9228-y.
237
238
239 FIGURE CAPTIONS
240

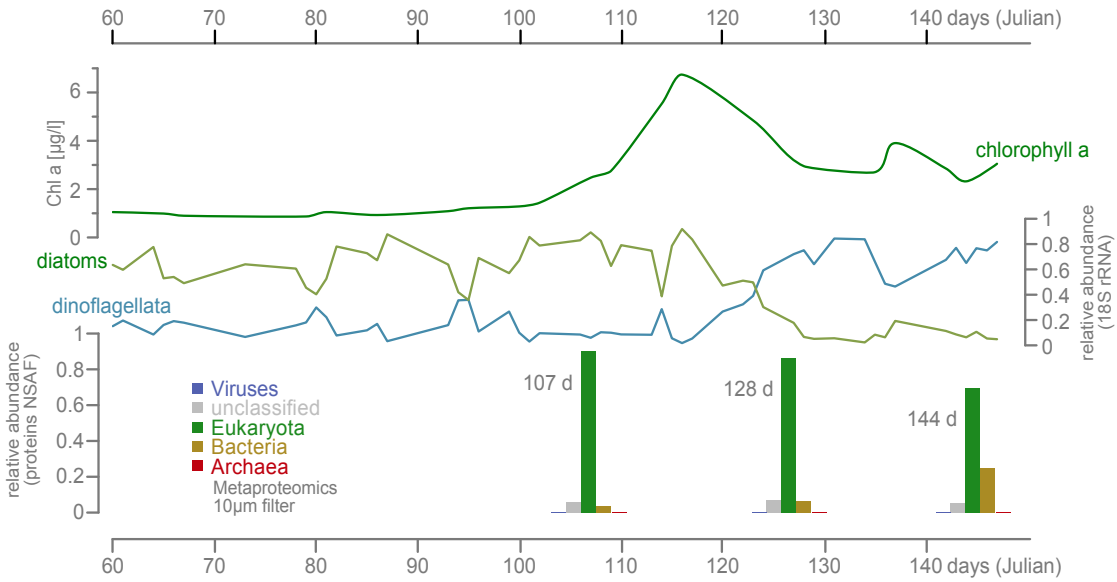

241
242
243 **Figure 1: Diatoms and dinoflagellates display opposing dynamics during the spring**
244 **phytoplankton bloom 2018.**

Particles larger than 10 µm were collected via filtration from 01 of March to 29 of May 2018 and microbial communities were analyzed using 16S and 18S rRNA gene amplicon sequencing and metaproteomics. Algal biomass (HPLC chlorophyll *a* measurements) peaked around the 26th of April (Julian day 116). Metaproteomics data from three selected timepoints displayed a dominance of eukaryotic proteins. Diatoms and dinoflagellates were the most abundant phytoplankton lineages as detected via 18S rRNA gene amplicon sequences and varied along the course of the bloom with dinoflagellates being more abundant after the chlorophyll *a* peak.

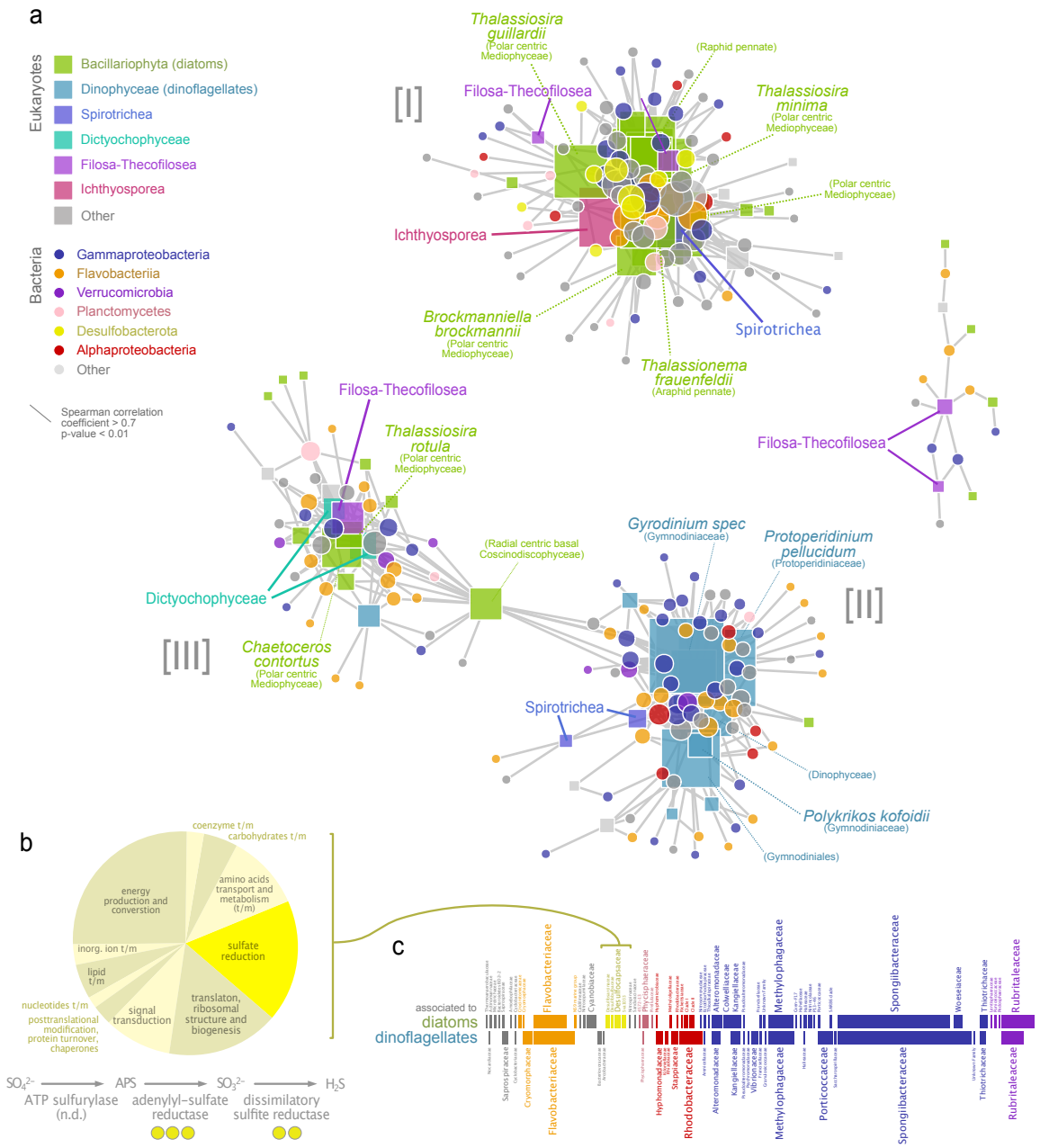

Figure 2: Diatoms distinctively co-occurred with *Desulfobacterota* and presence of key enzymes of the sulfur cycle was confirmed by metaproteomics.

a) A network analysis of 18S rRNA and 16S rRNA gene ASV co-occurrences resulted in two major network modules containing diatom [I] and dinoflagellate [II] 18S ASVs, respectively, as well as one mixed module [III]. The network was calculated based on Spearman correlations ($r > 0.7$, $p < 0.01$) between 18S ASVs and 16S ASVs exclusively. Several bacterial groups (circles) were associated with all modules, yet *Desulfobacterota* (yellow) were only associated with the diatom-dominated module. The sizes of the symbols correspond to the number of significant correlations of the nodes (degree). b) The bacterial ASVs temporally associated with diatoms and dinoflagellates represented distinct taxa. *Desulfobacterota* (yellow) as well as potentially sulfur-oxidizing *Ectothiorodospiraceae* were positively associated with diatoms but not with dinoflagellates. c) The pie chart displays relative abundances for all 22 protein groups classified as belonging to *Desulfobacterota* during all three timepoints sampled for metaproteomics. Proteins involved in sulfate reduction made up 18% of the metaproteome fraction (based on NSAF values, or 5 of 22 (23%) of proteins) assigned to *Desulfobacterota*. Of these, five protein groups represented enzymes involved in dissimilatory sulfate reduction (yellow circles). n.d. = not detected.

Supplementary information

Supplementary information 11
Supplementary methods 12
Supplementary figures 14
Supplementary table 19
Supplementary references 19

Supplementary methods

Sampling and filtration

For 16S and 18S rRNA gene amplicon sequencing and metagenome analysis, 40 L of subsurface seawater (1 m depth) were sampled in the morning at near daily intervals between beginning of March and end of May in 2018 at the station "Kabeltonne" (50° 11.3' N, 7° 54.0' E) near Helgoland in the south-eastern North Sea. Plankton biomass from 1 L of seawater was filtered using 10 µm pore size polycarbonate membrane filters (47 mm diameter, Millipore, Schwalbach, Germany) to separate PA microbes from smaller bacterial fractions. For metaproteomics analysis, 100 - 140 L of subsurface seawater were sampled at three selected timepoints during the bloom (Julian days 107, 128 and 144, representing early-, mid- and late bloom phases) and filtered onto 10 µm polycarbonate membrane filters (142 mm diameter, Millipore). In order to maximize biomass harvest while avoiding clogging, filtered volumes varied between 15 and 30.5 L per filter.

rRNA gene amplicon sequencing

For amplicon sequencing, a total of 51 samples were collected and analyzed. DNA was extracted from the filters using the Qiagen DNeasy Power soil Pro kit (Qiagen, Hilden, Germany) according to the manufacturer's instructions. Dislocation of microbial cells from the filters and mechanical lysis were achieved by bead beating in a FastPrep 24 5G (MP Biomedicals, Irvine, CA, USA). DNA concentrations were measured at a Qubit 3.0 fluorometer (Invitrogen, Carlsbad, CA, USA). Extracted DNA was amplified with primer pairs targeting the V4 region of the 16S rRNA gene [515f: 5 -GTGYCAGCMGCCGCGGTAA-3 , 806r: 5 -GGACTACNVGGGTWTCTAAT-3' (Walters et al., 2016)] and the V7 region of the 18S rRNA gene [F-1183mod: 5'-AATTTGACTCAACRCGGG-3', R-1443mod: 5'-GRGCATCACAGACCTG-3'] (Ray et al. 2016) coupled to custom adaptor-barcode constructs. PCR amplification and Illumina MiSeq (Illumina, San Diego, CA, USA) library preparation and sequencing (V3 chemistry) was carried out by LGC Genomics (LGC Genomics,Berlin, Germany).

Sequence reads free of adaptor and primer sequence remains were processed using the DADA2 package in R (version 1.2.0, Callahan et al., 2016). In summary, forward and reverse Illumina MiSeq reads were truncated to 200 bp, filtered (maxEE = 2, truncQ = 2, minLen = 175), dereplicated and error rates were estimated using the maximum possible error estimate from the data as an initial guess. Sample sequences were inferred, paired forward and reverse reads were merged and chimeric sequences were removed using the removeBimeraDenovo function. The resulting amplicon sequence variants (ASVs) were taxonomically classified using the Silva database (nr 99 v 138.1) for 16S rRNA and the PR2 database (version 4.13, minboot: 50) for 18S rRNA using the build-in RDP classifier. 16S rRNA gene amplicon reads classified as chloroplasts and mitochondria, as well as 18S rRNA gene reads classified as *Metazoa* (Zooplankton) were removed prior to the downstream analyses.

Co-occurrence networks were generated in R using Spearman rank correlation, as described previously (Bengtsson et al. 2017, correlation coefficient >0.7, adjusted p<0.01). We considered exclusively correlations between 18S and 16S ASVs and the final network was plotted using the igraph R package.

Construction of a metagenome-based database

332 Illumina sequencing was performed at the Max Planck Genome Centre Cologne on extracted
333 DNA using the HiSeq 2500 platform and 2 x 150 bp chemistry. Filtration and trimming of reads
334 were done as described previously (Francis et al. 2021). Read quality for each sample was
335 confirmed using FastQC v0.11.9 (Andrews 2014). Assembly was performed with MEGAHIT
336 v1.2.9 (Li et al. 2015) (kmer length: 21). Contigs below 2.5 kbp were removed using anvi-
337 script-reformat-fasta from within Anvi'o v6.2 (Eren et al. 2015). Genes were predicted using
338 Prodigal v2.6.3 (Hyatt et al. 2010) as implemented in the Prokka v1.11 annotation pipeline
339 (Seemann et al. 2014). These genes sequences were subsequently combined with a list of
340 common contaminants to generate a database for peptide-spectrum-matching (PSM) after
341 elimination of redundant sequences (97% redundancy) with CD-Hit (Fu et al. 2012, Li and
342 Godzik 2006).
343
344 **Metaproteomics**
345 Proteins were extracted from the filters of the 17th of April, 8th of May and 24th of May 2018
346 (Julian days 107, 128 and 144) as described previously (Schultz et al. 2020, Schultz 2022) and
347 analyzed with liquid chromatography-tandem mass spectrometry in triplicates. Briefly,
348 proteins were extracted from the filters via bead-beating followed by acetone precipitation.
349 The extracts were separated and fractionated by 1D SDS-PAGE and in-gel trypsin digested.
350 After desalting and concentration of the peptides using C18 Millipore® ZipTip columns,
351 samples were measured with an Orbitrap Velos™ mass spectrometer (ThermoFisher
352 Scientific, Waltham, MA, USA). After conversion into mgf file format using MS convert in
353 ProteoWizard (Palo Alto, CA, USA), spectra were matched against a metagenome-based
354 database containing 14,764,755 entries. Mascot (Matrix Science, London, UK) and Scaffold
355 (Proteome Software, Portland, OR, US) were used for peptide-spectrum-matching, protein
356 identification and protein grouping. Instead of setting an FDR-threshold, identification of
357 protein groups was based on number of peptide matches with a minimum of two, a protein
358 threshold of 99% and a peptide threshold of 95%. Identified protein groups were annotated
359 via Prophane v6.2.3 (Schiebenhoefer et al., 2020), using the Uniprot-TrEMBL (as of September
360 2021) and NCBI nr (as of February 2022) databases for taxonomic and EggNog v5.0.2 and
361 Tigrfams 15 databases for functional annotation with Prophane default settings. Relative
362 abundances were calculated as Normalized Spectral Abundance Factor (NSAF) values using
363 the quantification method "max_nsaf" integrated in Prophane (Schiebenhoefer et al., 2020).
364 Briefly, SAF values were calculated by dividing exclusive unique spectrum counts for each
365 protein group by protein length of the longest sequence in that protein group. For
366 normalization, SAF values were then divided by the sum of all SAF values of the sample.
367

Supplementary figures

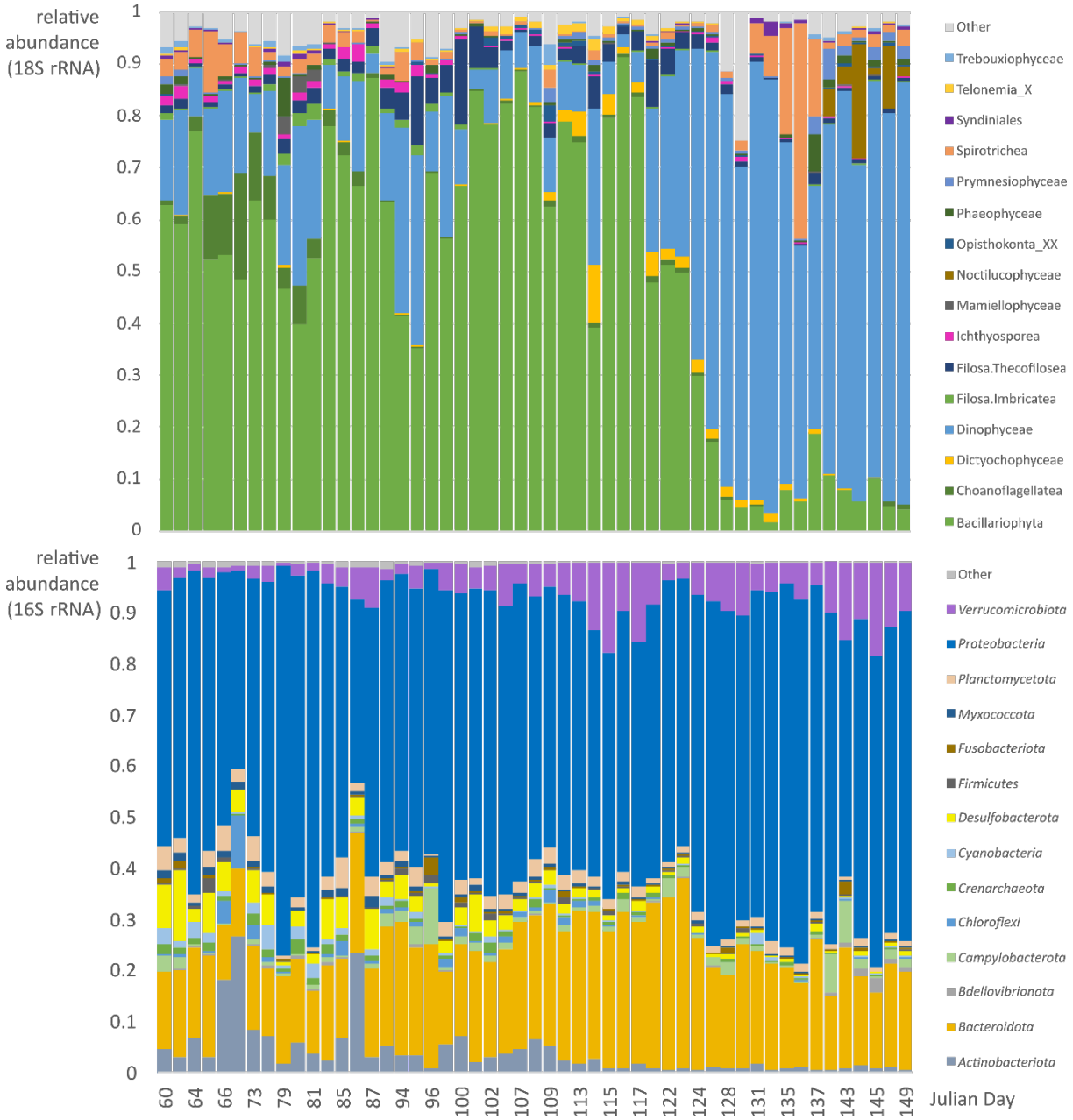

Fig. S1 SSU rRNA gene amplicon sequencing reveals taxonomic shifts during the course of the bloom. Eukaryote phylum distribution via 18S rRNA gene amplicon sequencing shows dominance of *Bacillariophyta* at the beginning of the phytoplankton bloom, shifting towards dominance of *Dinophyceae* in the last third of the surveillance period. 16S rRNA gene amplicon data revealed *Proteobacteria* and *Bacteroidota* as abundant bacterial phyla during the course of the phytoplankton bloom. Chloroplast and mitochondria sequence variants were removed from the 16S rRNA gene dataset prior to normalization.

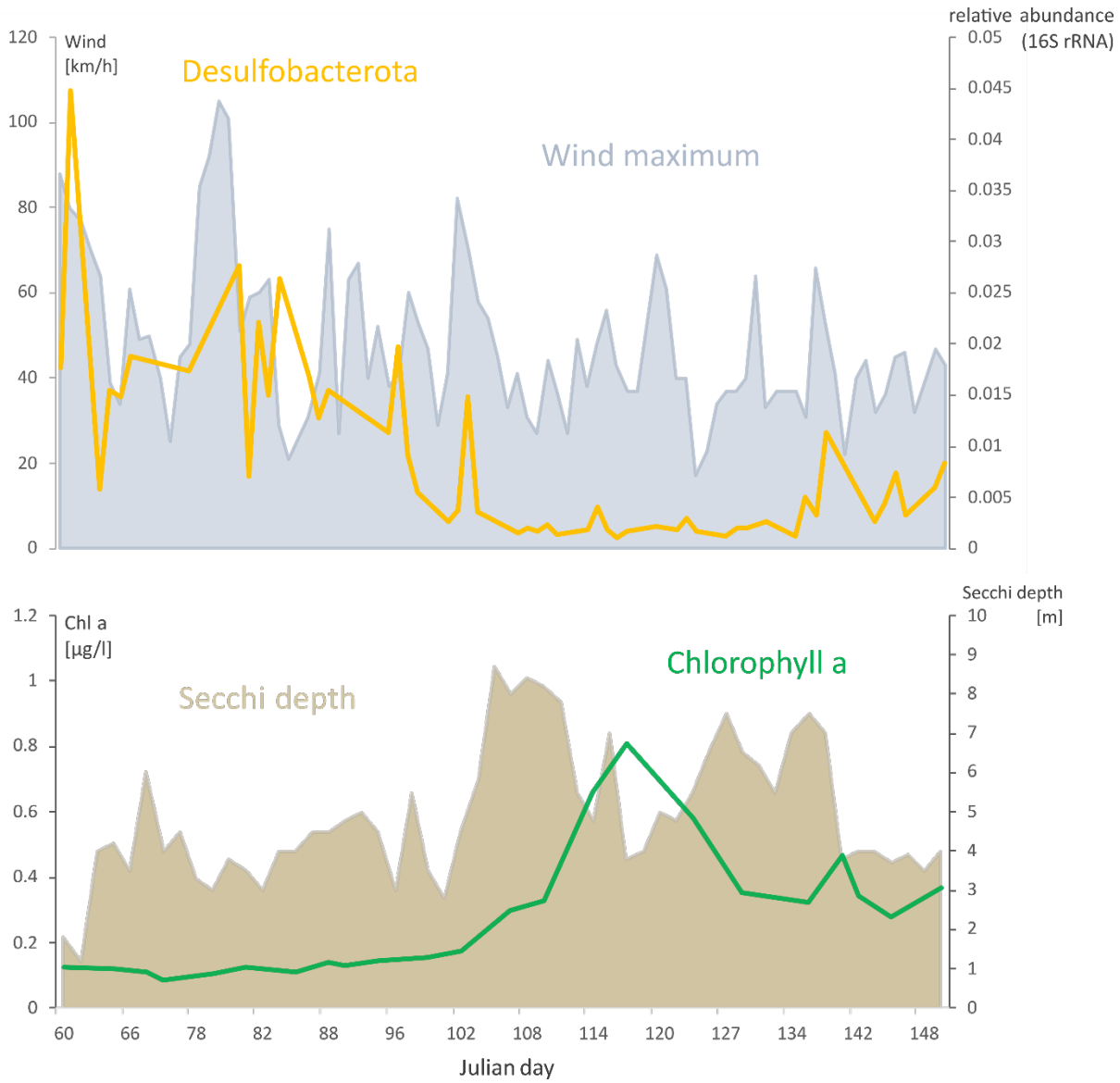

Fig. S2 Relative abundance of *Desulfobacterota* in relation to wind conditions (a), Secchi depth and chlorophyll *a* levels (b) during the 2018 spring bloom. Relative abundances of *Desulfobacterota* are based on 16S rRNA gene amplicon ASVs. Wind maxima are based on DWD Helgoland station via wetterkontor.de.

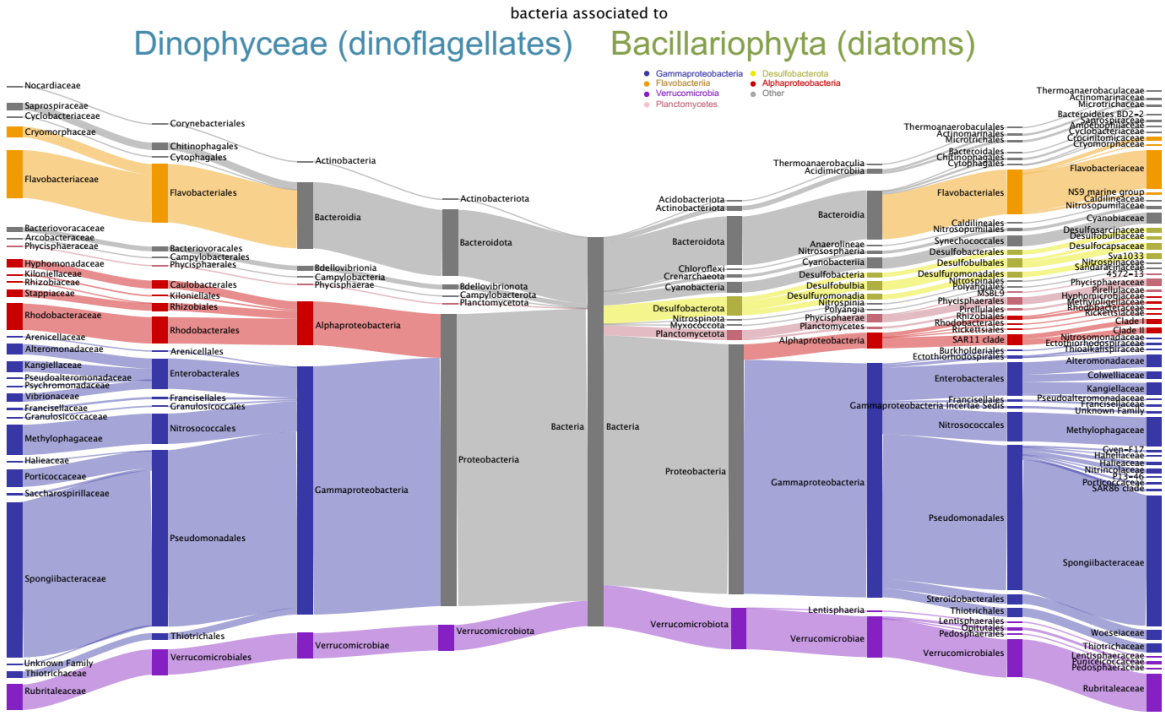

Fig. S3 Association of *Desulfobacterota* and *Ectothiorodospiraceae* with diatoms. Distribution of bacterial ASVs based on 16S rRNA gene amplicon data. Temporal associations to diatoms and dinoflagellates were taxonomically distinct.

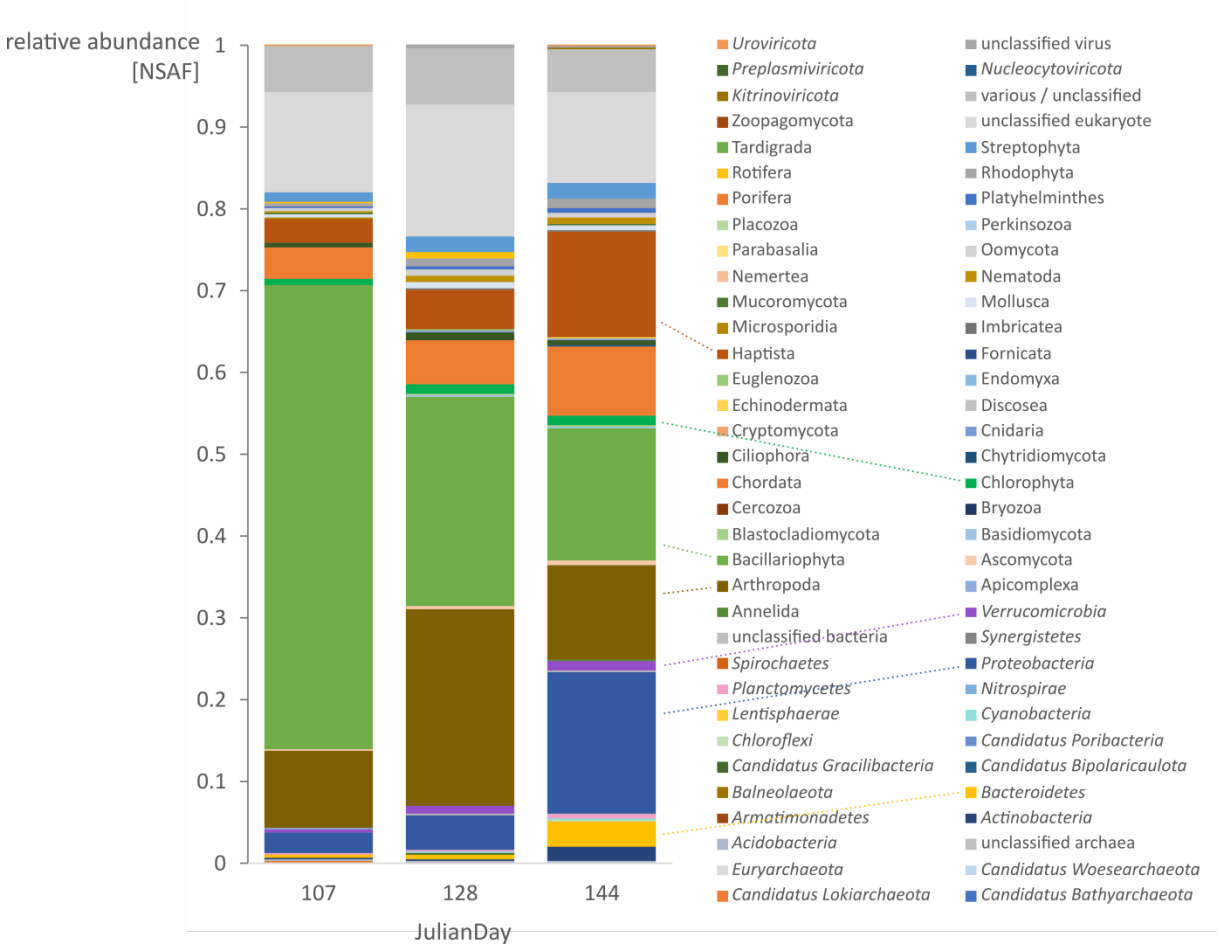

Fig. S4 Taxonomic distribution as detected by metaproteome analysis. Annotation based on the Trembl database of September 2021. Strong dominance of Bacillariophyta shifts towards increased abundance of bacterial proteins and especially *Proteobacteria* over time. Dinophyceae could not be identified using NR or Trembl, which reflects an underrepresentation of annotated dinoflagellate genome sequences in public databases, making peptide-spectrum-matching challenging.

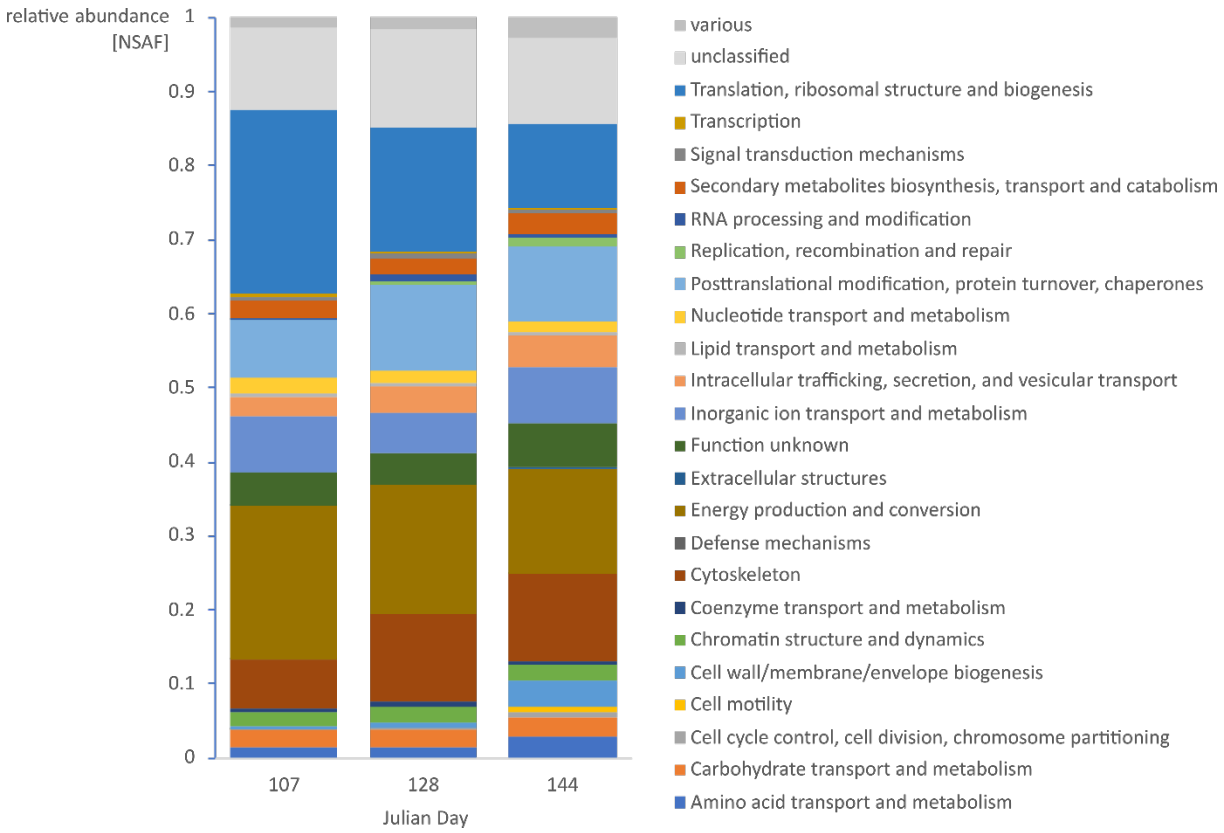

Fig. S5 Protein functions as detected by metaproteomics. Annotation was performed using EggNog v5.0.2 via Prophane. Metaproteome analysis was performed for three timepoints.

Supplementary table

Table T1 Five key enzymes associated with the sulfur cycle detected with metaproteomics. Adenylylsulfate-reductase and dissimilatory sulfite reductase assigned to three *Desulfobacterota* species could be detected. Functional annotation was based on EggNog v5.0.2, and the assignment of taxonomy was based on Swissprot (as of Sept. 2021), Trembl (as of Sept. 2021), and NCBI nr (as of Feb. 2022) database annnotations

#pg	type	NSAF			Tax_summary
		Julian Day 107	Julian Day 128	Julian Day 144	
112		0	0	0.00016602	*Desulfobublaceae* sp.
140		0	0	0.00049134	*Sorangium cellulosum*
182	Adenylylsulfate reductase	0	0	0.00015253	*Desulfobublaceae* sp.
239		0.0002743	7.6347E-05	0.00030024	*Anaeromyxobacter* sp. (strain Fw109-5)
293		5.7524E-05	7.7272E-05	0	*Desulfosarcina alkanivorans*
411		0	0	0.00025035	*Desulfosarcina alkanivorans*
440	Dissimilatory sulfite reductase	0	0	0.00013727	*Desulfovibrio vulgaris*
540		0.00023951	0	0	*Desulfobulbaceae* sp.
576	Dissimilatory sulfite reductase	0	0	0.00018468	*Desulfovibrio vulgaris*
666		0	0	0.00015508	*Wolinella succinogenes*
743		5.4294E-05	1.8454E-05	8.2017E-05	*Geobacter uraniireducens*
810		0.0002416	0.00015172	0.00011497	*Desulfatibacillum aliphaticivorans*
954		0	0	0.00016176	*Desulfurivibrio alkaliphilus*
960		0	0.00017834	0.00034704	*Desulfobacterales* sp.
1214		0	0	8.941E-05	*Desulfatibacillum aliphaticivorans*
1321		0	0.00010197	0.00015095	*Desulfosarcina alkanivorans*
1513		0	0	0.00011631	*Wolinella succinogenes*
2117		0	0	0.00026687	*Desulfobacterales* sp.
2147	Adenylylsulfate reductase	0	0	0.00037822	*Desulfopila inferna*
2297		0	2.6317E-05	4.2269E-05	*Deltaproteobacteria* sp.
2745		0	0	0.00026719	*Desulfobulbaceae* sp.
2868	Adenylylsulfate reductase	0	0	0.00011735	*Desulfobulbaceae* sp.

Supplementary references

410
411 Andrews S, FastQC: a quality control tool for high throughput sequence data. 2014. Available online
412 at: https://www.bioinformatics.babraham.ac.uk/projects/fastqc/ (accessed April 03, 2023).
413 Bengtsson MM, Bühler A, Brauer A, Dahlke S, Schubert H, Blindow I. Eelgrass Leaf Surface
414 Microbiomes Are Locally Variable and Highly Correlated with Epibiotic Eukaryotes. Front
415 Microbiol. 2017;8:1312. doi:10.3389/fmicb.2017.01312.
416 Callahan BJ, McMurdie PJ, Rosen MJ, Han AW, Johnson AJA, Holmes SP. DADA2: High-
417 resolution sample inference from Illumina amplicon data. Nat Methods.
418 2016;13(7):581–3. doi:10.1038/nmeth.3869.
419 Eren AM, Esen ÖC, Quince C, Vineis JH, Morrison HG, Sogin ML, Delmont TO. Anvi'o: an
420 advanced analysis and visualization platform for 'omics data. PeerJ. 2015;3:e1319.
421 doi:10.7717/peerj.1319.
422 Francis TB, Bartosik D, Sura T, Sichert A, Hehemann J-H, Markert S, et al. Changing
423 expression patterns of TonB-dependent transporters suggest shifts in polysaccharide
424 consumption over the course of a spring phytoplankton bloom. ISME J.
425 2021;15(8):2336–50. doi:10.1038/s41396-021-00928-8.
426 Fu L, Niu B, Zhu Z, Wu S, Li W. CD-HIT: accelerated for clustering the next-generation
427 sequencing data. Bioinformatics. 2012;28(23):3150–2.
428 doi:10.1093/bioinformatics/bts565.
429 Hyatt D, Chen G-L, Locascio PF, Land ML, Larimer FW, Hauser LJ. Prodigal: prokaryotic gene
430 recognition and translation initiation site identification. BMC Bioinformatics.
431 2010;11:119. doi:10.1186/1471-2105-11-119.
432 Li D, Liu C-M, Luo R, Sadakane K, Lam T-W. MEGAHIT: an ultra-fast single-node solution for
433 large and complex metagenomics assembly via succinct de Bruijn graph. Bioinformatics.
434 2015;31(10):1674–6. doi:10.1093/bioinformatics/btv033.
435 Li W, Godzik A. Cd-hit: a fast program for clustering and comparing large sets of protein or
436 nucleotide sequences. Bioinformatics. 2006;22(13):1658–9.
437 doi:10.1093/bioinformatics/btl158.
438 Ray JL, Althammer J, Skaar KS, Simonelli P, Larsen A, Stoecker D, et al. Metabarcoding and
439 metabolome analyses of copepod grazing reveal feeding preference and linkage to
440 metabolite classes in dynamic microbial plankton communities. Mol Ecol.
441 2016;25(21):5585–602. doi:10.1111/mec.13844.
442 Schiebenhoefer H, Schallert K, Renard BY, Trappe K, Schmid E, Benndorf D, et al. A complete
443 and flexible workflow for metaproteomics data analysis based on
444 MetaProteomeAnalyzer and Prophane. Nat Protoc. 2020;15(10):3212–39.
445 doi:10.1038/s41596-020-0368-7.
446 Schultz D, Zühlke D, Bernhardt J, Francis TB, Albrecht D, Hirschfeld C, et al. An optimized
447 metaproteomics protocol for a holistic taxonomic and functional characterization of
448 microbial communities from marine particles. Environ Microbiol Rep. 2020;12(4):367–
449 76. doi:10.1111/1758-2229.12842.
450 Schultz, D. (2022). Mechanisms of polysaccharide degradation of particle-associated
451 microbial communities. PhD thesis, University of Greifswald.
452 Seemann T. Prokka: rapid prokaryotic genome annotation. Bioinformatics.
453 2014;30(14):2068–9. doi:10.1093/bioinformatics/btu153.
454 Teeling H, Fuchs BM, Becher D, Klockow C, Gardebrecht A, Bennke CM, et al. Substrate-
455 controlled succession of marine bacterioplankton populations induced by a
456 phytoplankton bloom. Science. 2012;336(6081):608–11. doi:10.1126/science.1218344.

457 Walters W, Hyde ER, Berg-Lyons D, Ackermann G, Humphrey G, Parada A, et al. Improved
458 Bacterial 16S rRNA Gene (V4 and V4-5) and Fungal Internal Transcribed Spacer Marker
459 Gene Primers for Microbial Community Surveys. mSystems 2016.
460 doi:10.1128/mSystems.00009-15.
461
462
463
464